Preparation, Magnetic Susceptibility, and Specific Heat on Interlanthanide Perovskites ABO_3 (A = La–Nd, B = Dy–Lu)

Kentaro Ito, Keitaro Tezuka, and Yukio Hinatsu

Division of Chemistry, Graduate School of Science, Hokkaido University, Sapporo 060-0810, Japan

The interlanthanide perovskites $LaHoO_3$, $LaErO_3$, $LaTmO_3$, $LaYbO_3$, $LaLuO_3$, $CeTmO_3$, $CeYbO_3$, $CeLuO_3$, $PrYbO_3$, and $PrLuO_3$ were prepared by the coprecipitation method. Their magnetic susceptibility measurements were carried out in the temperature range between 1.8 and 300 K, and it was found that $LaYbO_3$, $CeYbO_3$, and $PrYbO_3$ had antiferromagnetic ordering with a weak ferromagnetism at 2.7 K. $LaErO_3$ also showed antiferromagnetic ordering at 2.4 K. Specific heat measurements for $LaErO_3$ and $LaYbO_3$ showed the λ-type anomaly at 2.4 and 2.7 K, respectively, which is in good agreement with the susceptibility measurements. © 2001 Academic Press

1. INTRODUCTION

The perovskite-type oxides have the general formula ABO_3 in which A represents a large cation and B represents a small cation. Figure 1 shows the crystal structure of an orthorhombically distorted perovskite-type oxide, $LaLuO_3$ (A = La, B = Lu). The perovskite structure can be described as a framework of corner-shared BO_6 octahedra that contain A cations at 12-coordinate sites. Since the B cations generally determine the physical properties of the ABO_3 perovskites, a large number of studies have been made on the perovskites that accommodate a variety of transition metal ions at their B sites. However, only a few studies have so far been made for the perovskites with lanthanide ions at their B sites because lanthanide ions tend to occupy the A sites for their large ionic radii.

Berndt *et al.* reported the preparation of interlanthanide perovskites $LaHoO_3$, $LaErO_3$, $LaTmO_3$, $LaYbO_3$, $LaLuO_3$, $CeTmO_3$, $CeYbO_3$, $CeLuO_3$, and $PrLuO_3$, containing two kinds of trivalent lanthanide ions at both the A and B sites (1). Moreau determined the effective magnetic moments of $LaLnO_3$ (Ln = Ho, Er, Tm, and Yb) from their magnetic susceptibility measurements (2). Moreau and co-workers also found that the Er spins in the $LaErO_3$ order antiferromagnetically at $T = 2.4$ K in a canted arrangement (3, 4). Except for these studies, the magnetic properties of

such interlanthanide perovskite compounds have not been studied.

In this study, we prepared a series of interlanthanide ternary oxides, $A^{3+}B^{3+}O_3$, with the perovskite structure and refined their crystal structures. Through magnetic susceptibility measurements, we will examine the magnetic properties of these complex oxides and elucidate the roles of A site ion and B site ion in the magnetic behavior.

2. EXPERIMENTAL

In this study, we prepared the samples by the coprecipitation method to accelerate the reaction rate. Ln_2O_3 (Ln = La, Nd, Dy–Lu), $Ce(NO_3)_3$, and Pr_6O_{11} were used as starting materials. La_2O_3 and Nd_2O_3 were heated in air at 800°C before use because of its hygroscopicity. These starting materials were weighed in correct composition ratios and dissolved in heated nitric acid. After this solution was cooled, aqueous ammonia was added to it to coprecipitate mixed hydroxides. The precipitate was percolated and heated in air or a hydrogen atmosphere at 1000–1500°C for several days with grinding at regular intervals until a single perovskite phase was obtained.

The powder X-ray diffraction profiles were measured at room temperature using a Rigaku RINT 2000 diffractometer with Cu$K\alpha$ radiation equipped with a curved graphite monochromator. The data were collected by step scanning in the angle range $10° \leq 2\theta \leq 120°$ with increments of 0.04° and counting time of 5 s step.

The temperature dependence of magnetic susceptibility was measured with a SQUID magnetometer (Quantum Design, MPMS) under both zero-field-cooled conditions (ZFC) and field-cooled conditions (FC). The former was measured upon heating the sample to 300 K under the applied magnetic field of 0.1 T after zero-field cooling to 1.8 K. The latter was measured upon cooling the sample from 300 to 1.8 K at 0.1 T. The magnetization was measured at 1.8 K in the magnetic field range $-5 \leq H \leq 5$ T.
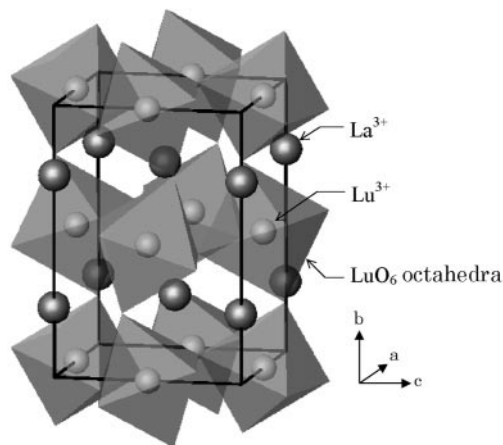
FIG. 1.   Crystal structure of LaLuO₃.

TABLE 1
Preparation Conditions for ABO_3 Perovskites

	B					
A	Dy	Ho	Er	Tm	Yb	Lu
La	—	1150°C 180 h in air	1400°C 36 h in air	1400°C 36 h in air	1400°C 36 h in air	1400°C 36 h in air
Ce	—	—	—	1250°C 652 h in H₂	1250°C 206 h in H₂	1250°C 48 h in H₂
Pr	—	—	—	—	1250°C 393 h in air	1250°C 72 h in air
Nd	—	—	—	—	—	—

Note. —: could not be prepared.

The specific heat was measured using a relaxation technique supplied by a commercially available specific heat measuring system (Quantum Design, PPMS) in the temperature range $1.8 \leq T \leq 300$ K. The sample in the form of a pellet (~ 10 mg) was mounted on an alumina plate with apiezon for better thermal contact.

3. RESULTS AND DISCUSSION

3.1. Results of Synthesis

The powder X-ray diffraction measurements show that LaHoO₃, LaErO₃, LaTmO₃, LaYbO₃, LaLuO₃, CeTmO₃, CeYbO₃, CeLuO₃, PrYbO₃, and PrLuO₃ were formed in a single perovskite phase. The results are summarized in Table 1. It is found that the compounds located at the upper right positions in Table 1, i.e., compounds containing larger lanthanide ions at the A site and smaller lanthanide ions at the B site, tend to be prepared easily. In contrast, the compounds located at the lower left positions in Table 1, where the ionic radius of the A site ion is comparable to that of the B site ion, could not be obtained in our preparation.

To discuss the stability of the perovskite-type compounds ABO_3, Goldschmidt introduced the tolerance factor (t) defined by $t = (r_A + r_O)/\sqrt{2}(r_B + r_O)$, where r_A, r_B, and r_O are the radii of the A and B ions and oxygen ions, respectively (5). Generally speaking, the perovskite structure occurs within the range of $0.75 \leq t \leq 1$. A tolerance factor less than unity
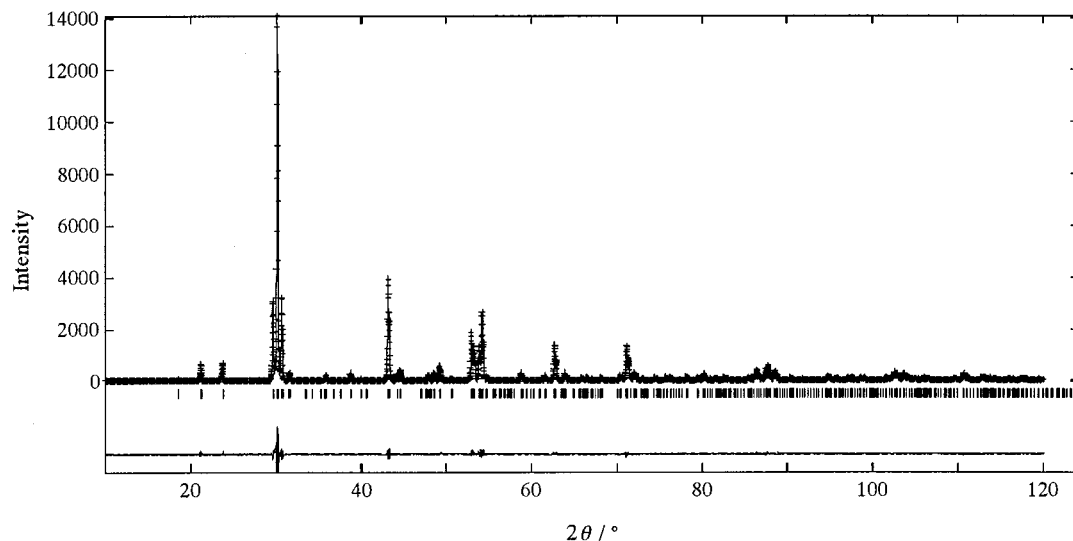

FIG. 2.   Powder X-ray diffraction pattern fitting for LaLuO₃. The calculated and observed patterns are shown on the top solid line and the cross markers, respectively. The vertical marks in the middle show positions calculated for Bragg reflections. The trace on the bottom is a plot of the difference between calculated and observed intensities.
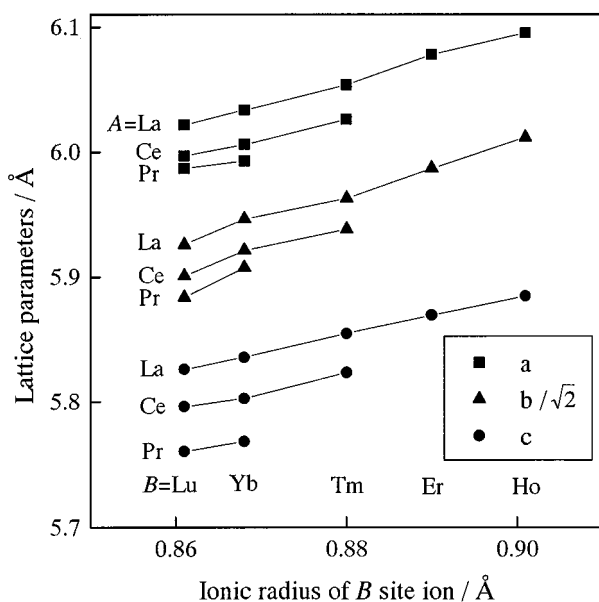
TABLE 2
Lattice Parameters and Reliability Factors R

Compounds	a (Å)	b (Å)	c (Å)	R_{wp}	R_p	R_I
LaHoO$_3$	6.0952(1)	8.5018(1)	5.8846(1)	14.19	9.45	2.96
LaErO$_3$	6.0780(1)	8.4667(1)	5.8694(1)	13.04	9.73	3.21
LaTmO$_3$	6.0537(1)	8.4327(1)	5.8547(1)	11.14	8.38	1.73
LaYbO$_3$	6.0336(1)	8.4094(1)	5.8357(1)	13.20	9.26	1.97
LaLuO$_3$	6.0218(1)	8.3804(1)	5.8259(1)	13.01	9.15	1.87
CeTmO$_3$	6.0263(1)	8.3978(2)	5.8234(1)	17.05	11.56	6.13
CeYbO$_3$	6.0062(1)	8.3740(1)	5.8026(1)	16.43	11.15	4.22
CeLuO$_3$	5.9969(1)	8.3447(1)	5.7964(1)	12.87	8.69	2.17
PrYbO$_3$	5.9929(1)	8.3547(1)	5.7684(1)	18.76	13.66	6.78
PrLuO$_3$	5.9868(1)	8.3204(1)	5.7603(1)	13.53	9.05	2.69

Note. $R_{wp} = [\sum w(|F(o)| - |F(c)|)^2 / \sum wF(o)^2]^{1/2}$, $R_p = \sum(|F(o)| - ||F(c)|)/\sum |F(o)|$, and $R_I = \sum |I_k(o) - I_k(c)|/\sum I_k(o)$.

signifies the perovskite structure distorting from the ideal cubic symmetry. For larger deviation from the ideal ionic radius ratio, the compound distorts more from the cubic symmetry. The values for the tolerance factors of the compounds prepared in this study indicate that a tolerance factor more than 0.843 is needed to prepare the present ABO_3 perovskites.

The compounds containing Ce^{3+} ions at the A sites required heating in a flow of hydrogen gas. Since the cerium ion has the tetravalent state in addition to the trivalent state, hydrogen reduction is essential in preparing compounds containing cerium ions in the trivalent state.

TABLE 3
Crystallographic Data for LaLuO$_3$

Atom	Site	x	y	z	B (Å^2)
La	$4c$	0.0507(3)	$\frac{1}{4}$	$-0.0138(6)$	0.2(1)
Lu	$4b$	$\frac{1}{2}$	0	0	0.1(1)
O(1)	$4c$	0.444(4)	$\frac{1}{4}$	0.121(5)	0.1(6)
O(2)	$8d$	0.307(3)	0.063(3)	0.693(3)	0.1(4)

Note. $a = 6.0218(1)$ Å, $b = 8.3804(1)$ Å, $c = 5.8259(1)$ Å.

3.2. Structural Properties

From Rietveld analysis with the computer program RIETAN-97 (6), all powder X-ray diffraction patterns for the samples having a single perovskite phase were indexed with the space group *Pnma*. They were formed in an orthorhombically distorted perovskite. The observed, calculated, and difference profiles of the powder X-ray diffraction for LaLuO$_3$, as a typical example, are plotted in Fig. 2. The resultant lattice parameters and reliability factors R are listed in Table 2. These lattice parameters are very close to those in the previous reports (1). Figure 3 shows the variation of lattice parameters with the ionic radius of the B site ion. They increase monotonously with the size of the B site ion.

Table 3 and Fig. 1 show the crystallographic data and the crystal structure for LaLuO$_3$ determined in this study, respectively. The corner-sharing LuO$_6$ octahedra form

FIG. 3. Variation of lattice parameters for ABO_3 perovskites with the ionic radius of the B site ion.
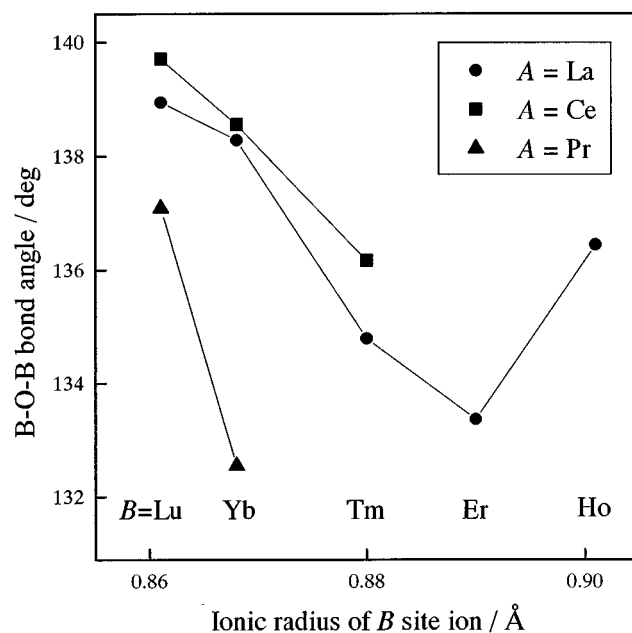
**FIG. 4.** Variation of B–O–B bond angles for ABO_3 perovskites with the ionic radius of the B site ion.

TABLE 4
Calculated Magnetic Moments for Ln^{3+} (p_{eff}), the Effective Magnetic Moments (μ_{eff}), and Weiss Constants (θ)

Compounds	p_{eff} (μ_B)	μ_{eff} (μ_B)	θ (K)
$LaHoO_3$	10.6	10.5	− 12.3
$LaErO_3$	9.58	9.36	− 10.4
$LaTmO_3$	7.56	7.31	− 29.1
$LaYbO_3$	4.54	4.80	− 130
$CeTmO_3$	7.98	8.01	− 33.3
$CeYbO_3$	5.20	6.02	− 188
$CeLuO_3$	2.54	2.52	− 86.9
$PrYbO_3$	5.78	5.85	− 75.4
$PrLuO_3$	3.58	3.49	− 16.5

a three-dimensional framework. The Lu–O–Lu bond angle considerably deviates from 180°, that is, $LaLuO_3$ distorts largely from the ideal cubic perovskite structure. The same situation is valid for the other compounds prepared in this study. Figure 4 shows the variation of B–O–B bond angles with the ionic radius of the B site ion. As the ionic radius of the B site ion increases, the B–O–B bond angle decreases, which means that the distortion of the crystal structure from the ideal cubic perovskite structure increases with the ionic radius of the B site ion.

3.3. Magnetic Properties and Specific Heats

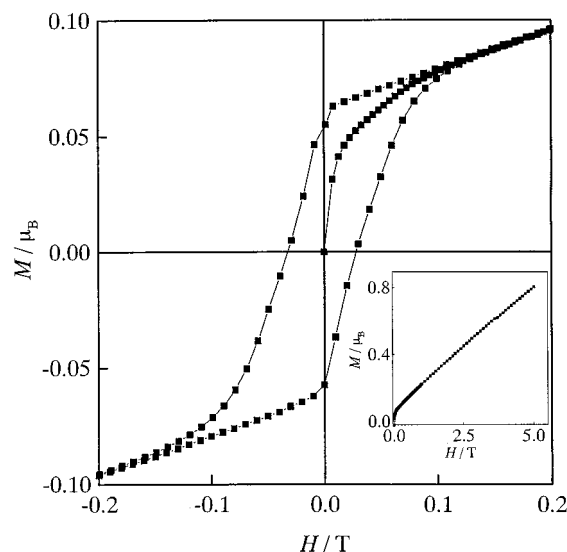From the magnetic susceptibility measurements, antiferromagnetic transitions have been observed for $LaErO_3$,
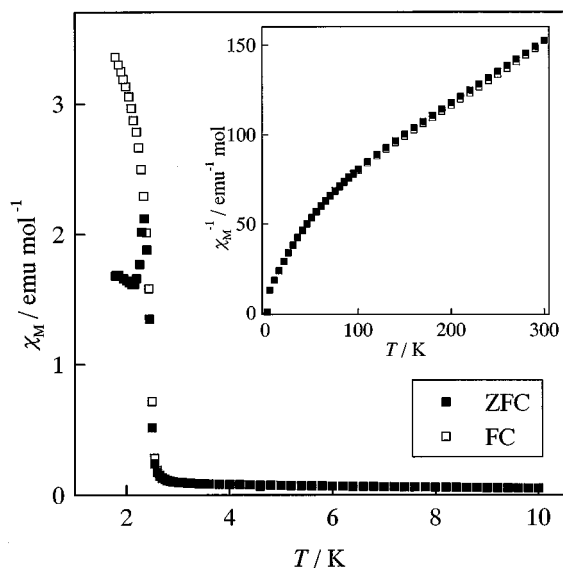
$LaYbO_3$, $CeYbO_3$, and $PrYbO_3$ at 2.4, 2.7, 2.7, and 2.7 K, respectively. Other compounds are paramagnetic down to 1.8 K. The effective magnetic moments μ_{eff} and Weiss constants θ calculated from the reciprocal magnetic susceptibility vs temperature curves are listed in Table 4. The magnetic hysteresis loops were found for $LaYbO_3$, $CeYbO_3$, and $PrYbO_3$ in their magnetization measurements.

3.3.1. $LaYbO_3$. Figure 5 shows the temperature dependence of magnetic susceptibility for $LaYbO_3$. It is found that an antiferromagnetic transition has been found at 2.7 K, and that a large divergence in the magnetic susceptibilities between the ZFC and the FC occurs below this temperature. Temperature dependence of the reciprocal magnetic susceptibility (the inset of Fig. 5) shows that the magnetic susceptibility in the higher temperature range can be fitted well by the Curie-Weiss law. The effective magnetic moment μ_{eff} is obtained to be 4.77 μ_B, which is in good agreement with the free ion value of Yb^{3+}, 4.54 μ_B. The deviation from the Curie–Weiss relation at low temperatures is considered to be due to the crystal field effect.

In order to investigate the magnetic transition in detail, the magnetization measurements were performed at 1.8 K. The results are shown in Fig. 6. The magnetic hysteresis loop is found, which indicates the existence of a ferromagnetic component in the magnetic properties of this compound. The hysteresis loop exists only in the range $H = -0.1$–0.1 T and it is rather small. We consider that a weak ferromagnetism associated with the antiferromagnetism is caused by the canted spin of Yb^{3+}.

FIG. 5. Temperature dependence of the magnetic susceptibility for $LaYbO_3$ at low temperatures. The inset shows the inverse magnetic susceptibility of $LaYbO_3$ as a function of temperature.

FIG. 6. Variation of magnetization with the applied magnetic field in the range $-0.2 \leq H \leq 0.2$ T at 1.8 K. The inset shows the magnetization in the range $0 \leq H \leq 5$ T.
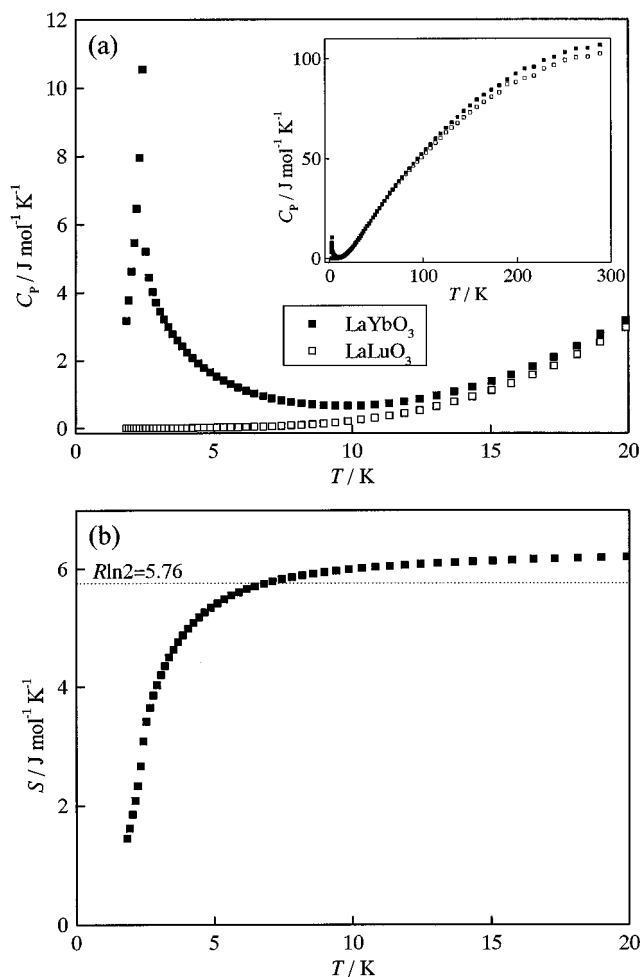
FIG. 7. (a) Temperature dependence of the specific heat of $LaYbO_3$. For comparison, the data for $LaLuO_3$ are also shown. (b) Magnetic entropy of $LaYbO_3$.

Figure 7a shows the variation of specific heat for $LaYbO_3$ as a function of temperature. A λ-type anomaly has been observed at 2.7 K, which corresponds to the magnetic anomaly found in the magnetic susceptibility. In the same figure, the results of the specific heat measurements for $LaLuO_3$, which has no paramagnetic ion, are also shown. If we assume that the electronic and lattice contributions to the specific heat are equal between $LaYbO_3$ and $LaLuO_3$, the magnetic specific heat for $LaYbO_3$ is obtained by subtracting the specific heat of $LaLuO_3$ from that of $LaYbO_3$. From its temperature dependence, the magnetic entropy change associated with the Yb^{3+} antiferromagnetic transition is calculated as shown in Fig. 7b. It is saturated around 10 K and its value is about 6, which is very close to $R \ln W = R \ln 2 = 5.76$, where R and W are a molar gas constant and a degree of degeneracy of the ground state, respectively. This result indicates that the degeneracy of the ground state should be a doublet. In an octahedral crystal field environment, the ground state of the Yb^{3+} ion (the

state $^2F_{7/2}$) is the Γ_6 doublet (7); i.e., the λ-type anomaly found for $LaYbO_3$ at 2.7 K is also ascribable to the Yb^{3+} antiferromagnetic transition.

3.3.2. $CeYbO_3$ and $PrYbO_3$. Figures 8a and 8b show the temperature dependencies of magnetic susceptibilities for $CeYbO_3$ and $PrYbO_3$, respectively. Both the compounds show quite similar magnetic behavior. The magnetic susceptibilities increase with decreasing temperature and they rapidly increase when the temperature is decreased through 2.7 K. At the same time, the divergence of the magnetic susceptibilities between the ZFC and the FC has been observed below this temperature. The Curie–Weiss law holds in the temperature range between 150 and 300 K. Very large negative Weiss constants θ found for both compounds indicate that the magnetic behavior below 2.7 K is antiferromagnetic. The existence of the small magnetic hysteresis loop has also been observed at 1.8 K from their magnetization measurements. These experimental results are quite
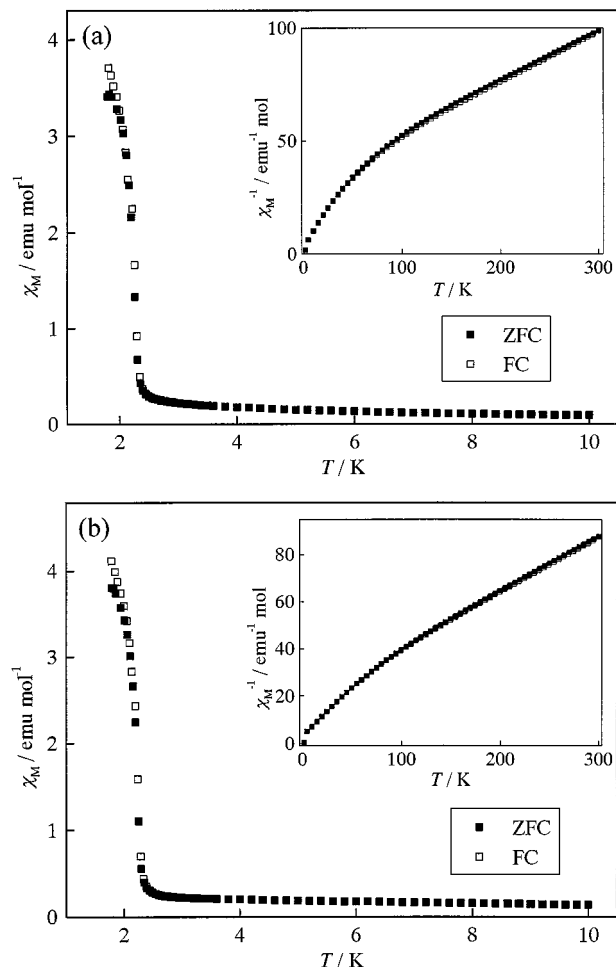

FIG. 8. Temperature dependence of the magnetic susceptibility for (a) $CeYbO_3$ and (b) $PrYbO_3$. The insets show the inverse magnetic susceptibilities.
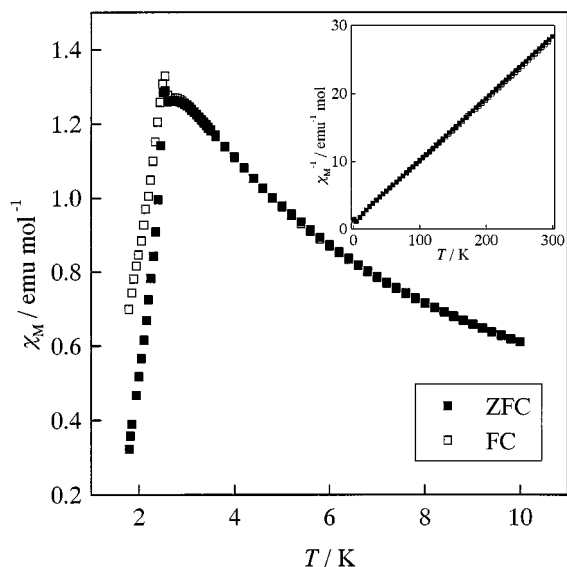
FIG. 9. Temperature dependence of the magnetic susceptibility for $LaErO_3$.

similar to those for $LaYbO_3$. Thus, we consider that the main magnetic interaction in $CeYbO_3$ and $PrYbO_3$ below 2.7 K is antiferromagnetic and that a weak ferromagnetism is also present.

3.3.3. LaErO₃. Figure 9 shows the temperature dependence of magnetic susceptibility for $LaErO_3$, indicating an antiferromagnetic ordering at 2.4 K. This result is consistent with that reported by Moreau *et al.* (3). No magnetic hysteresis loop has been observed, even at 1.8 K from the magnetization measurements.

Figure 10a shows the variation of specific heat for $LaErO_3$ with temperature. The specific heat anomaly has been observed at 2.4 K, which corresponds to the onset of antiferromagnetic ordering found in the magnetic susceptibility. A divergence of the specific heats between $LaErO_3$ and $LaLuO_3$ above 10 K is considered to be due to the Schottky's specific heats. In the same way as the case for $LaYbO_3$, the magnetic specific heat for $LaErO_3$ is obtained by subtracting the specific heat of $LaLuO_3$ from that of $LaErO_3$, and the magnetic entropy change associated with the Er^{3+} antiferromagnetic ordering is also calculated as shown in Fig. 10b. It is saturated around 10 K and its value is 5.5, which is very close to $R \ln 2 = 5.76$. This result indicates that the degeneracy for the ground state should be a doublet. The ground state of $^4I_{15/2}$ for the Er^{3+} ion is a quartet state Γ_8 or a doublet state Γ_7 in an octahedral crystal field environment (7). As described already, the crystal symmetry for $LaErO_3$ is not cubic, but orthorhombic; i.e., the crystal field symmetry around the Er^{3+} ion should be lower than the ideal octahedral one. Then, the ground state is no longer the quartet state Γ_8; i.e., it is a doublet. Therefore, the anomaly found
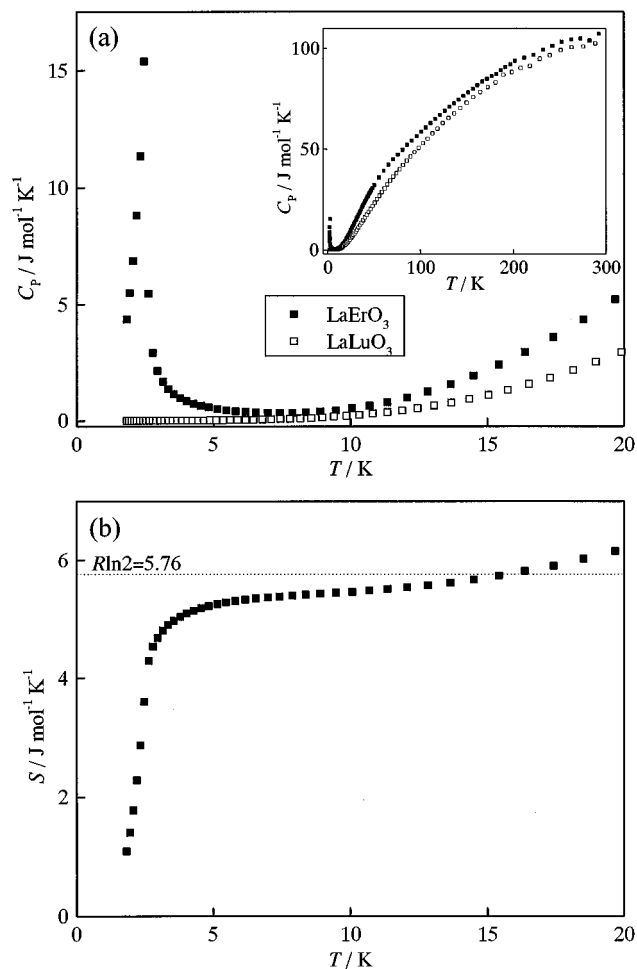

FIG. 10. (a) Temperature dependence of the specific heat of $LaErO_3$. For comparison, the data for $LaLuO_3$ are also shown. (b) Magnetic entropy of $LaErO_3$.

for $LaErO_3$ is considered to be due to the Er^{3+} antiferromagnetic transition.

4. CONCLUSION

Table 5 summarizes the magnetic properties of the ABO_3-type compounds prepared in this study. Any compound containing Er^{3+} or Yb^{3+} at the B sites shows the antiferromagnetic transition at very low temperatures. The compounds containing Yb^{3+} ions at the B sites $AYbO_3$ (A = La, Ce, and Pr) show very similar magnetic behavior, indicating that the magnetic properties of these compounds are independent of the A site ions and that they are mainly due to the behavior of the B site ions in the perovskites.

Since the Er^{3+} and Yb^{3+} ions are both Kramers' ions having odd unpaired electrons, the ground states of these ions are degenerate, even in a crystal field with low symmetry. This means that magnetic cooperation phenomena

TABLE 5
Magnetic Properties for ABO_3 Perovskites

				B		
A	Dy	Ho	Er	Tm	Yb	Lu
La	—	para	antiferro $T_N = 2.4$ K	para	antiferro $T_N = 2.7$ K	dia
Ce	—	—	—	para	antiferro $T_N = 2.7$ K	para
Pr	—	—	—	—	antiferro $T_N = 2.7$ K	para
Nd	—	—	—	—	—	—

Note. antiferro: antiferromagnetic; para: paramagnetic; dia: diamagnetic; and —: could not be prepared.

due to interactions between these Kramers' ions can be observed at very low temperatures, which is consistent with the present experimental results.

REFERENCES

1. U. Berndt, D. Maier, and C. Keller, *J. Solid State Chem.* **13,** 131 (1975).
2. J. M. Moreau, *Mater. Res. Bull.* **3,** 427 (1968).
3. J. M. Moreau, J. Mareschal, and E. F. Bertaut, *Solid State Commun.* **6,** 751 (1968).
4. J. Mareschal, J. M. Moreau, G. Ollivier, P. Pataud, and J. Sivardiere, *Solid State Commun.* **7,** 1669 (1969).
5. V. M. Goldschmidt, *Str. Nor. Vidensk-Akad. Oslo* **1,** 1 (1926).
6. F. Izumi, *Nippon Kesshou Gakkaishi* **27,** 23 (1986).
7. K. R. Lea, M. J. M. Leask, and W. P. Wolf, *J. Phys. Chem. Solids* **23,** 1381 (1962).
8. R. D. Shannon, *Acta Crystallogr. A* **32,** 751 (1976).